Estuarine, Coastal and Shelf Science 343 (2026) 110297

Contents lists available at ScienceDirect

Estuarine, Coastal and Shelf Science

journal homepage: www.elsevier.com/locate/ecss

Monitoring aquaculture pond expansion as a driver of mangrove loss in coastal Asia

Marco Ottinger [a,*], Luis David Almeida Famada [b], Juliane Huth [a]

[a] German Aerospace Center (DLR), Earth Observation Center (EOC), German Remote Sensing Data Center (DFD), Germany
[b] University of Wuerzburg, Institute of Geography and Geology, Department of Remote Sensing, Germany

ARTICLE INFO

Keywords:
Mangrove ecosystems
Pond aquaculture
Aquaculture expansion
Mangrove loss
Earth observation
Satellite time series
Coastal management
Asia

ABSTRACT

Mangrove ecosystems provide essential services for biodiversity, coastal protection, and carbon sequestration, yet they remain under pressure due to the expansion of pond-based aquaculture. In this study, we quantify the direct contribution of pond aquaculture expansion to mangrove loss at large spatial and temporal scale using integrated Earth observation data from 1996 to 2019. We combine a continental-scale aquaculture pond time series derived from Landsat and Sentinel time series with mangrove extent data from the Global Mangrove Watch. To enable robust attribution despite uneven temporal sampling, we introduce a harmonized positional time-index framework that aligns pond activation with episodic mangrove observations. Mangrove loss is conservatively attributed to aquaculture when disappearance occurs at or shortly after pond activation. By overlaying and comparing these datasets at the country level, we identified instances of direct conversion and tracked changes over time. Our temporal analysis of pond-activation–attributed mangrove loss across twelve Asian countries reveals a highly regionalized pattern of aquaculture-driven mangrove conversion. The largest losses occurred during the early phase from 1996 to 2007, dominated by Indonesia (13,046 ha) and Myanmar (2892 ha). Although losses declined after 2007 in most countries, Indonesia and Myanmar continued to experience substantial mangrove conversion during later periods, while other countries showed only minor changes after 2010. Spatial analyses identify clear hotspots where dense pond clusters coincide with historic mangrove degradation. Overall, our results on aquaculture-driven mangrove loss in Asia highlight a pronounced spatial concentration of mangrove conversion driven primarily by a few countries and distinct periods of intensified land-use change, particularly linked to aquaculture expansion. The proposed framework improves causal inference in multi-source satellite analyses and supports more informed coastal management and conservation strategies.

1. Introduction

1.1. Mangrove ecosystems under pressure from pond aquaculture expansion

Mangroves are among the most valuable and productive ecosystems on Earth, playing a crucial role in maintaining environmental balance and supporting both human and natural systems (Friess et al., 2019; Kuenzer et al., 2011). Ecologically, mangroves provide critical habitat for a wide variety of species. Their complex root systems offer shelter and breeding grounds for fish, crustaceans, birds, and other wildlife. This biodiversity supports not only marine and coastal food chains but also local fisheries that many coastal communities rely on for their livelihoods (Vo et al., 2012). Mangroves also function as natural coastal defenses. Their dense root networks stabilize shorelines, reduce erosion, and absorbed wave energy, particularly during tropical storms and storm surges, thereby helping to prevent coastal flooding (Spalding et al., 2014). These protective services are increasingly vital in the context of climate change and rising sea levels (Jennerjahn et al., 2017; Schuerch et al., 2018). In addition, mangroves are highly efficient carbon sinks, sorting large amount of carbon dioxide in both above-ground biomass and organic-rich soils, thereby contributing to climate mitigation (Akram et al., 2023; Chatting et al., 2024; Lagomasino et al., 2019; Zhang et al., 2024). Beyond their ecological and protective functions,

This article is part of a special issue entitled: YECSS_Coastal remote sensing published in Estuarine, Coastal and Shelf Science.

* Corresponding author.
E-mail address: marco.ottinger@dlr.de (M. Ottinger).

https://doi.org/10.1016/j.ecss.2026.110297
Received 21 January 2026; Received in revised form 6 August 2026; Accepted 30 September 2026
Available online 6 October 2026
0272-7714/© 2026 Published by Elsevier Ltd.

mangroves improve coastal water quality by filtering pollutants and trapping sediments and they provide resources such as timber, fuel, and traditional medicines. Protecting and restoring mangrove ecosystems is therefore essential—not only for preserving biodiversity and coastal resilience but also for mitigating climate change and supporting sustainable development (Akram et al., 2023; Rodríguez-Rodríguez et al., 2025; Romañach et al., 2018).

Despite their value, mangroves are under increasing pressure from human activities. In 2020, global mangrove cover was around 14.8 million hectares, with a net loss of 284 thousand hectares between 2000 and 2020 (FAO, 2023), driven primarily by aquaculture expansion, natural retraction, and oil palm conversion. Asia contains approximately 40 percent (6 million hectares) of the world's mangroves. Pond-based aquaculture, particularly shrimp and fish farming, is concentrated in low-lying coastal zones, where brackish water and flat terrain favor pond construction. However, the construction of pond aquaculture frequently involves the clearing of mangroves, making aquaculture one of the leading drivers of mangrove deforestation in Southeast Asia and other tropical regions (Hagger et al., 2022; Leal and Spalding, 2024). Countries such as Thailand, Vietnam, Indonesia, and Ecuador have experienced extensive mangrove conversion to aquaculture ponds (Arifanti et al., 2022a, 2022b; Aslan et al., 2021). This transformation eliminates biodiversity-rich habitats (Polidoro et al., 2010) and weakens natural coastal protection, increasing vulnerability to erosion, storm surges, and saline intrusion, threatening both environmental health and the safety of local communities (Akram et al., 2023; Kuenzer et al., 2011). Moreover, aquaculture in former mangrove areas results in unsustainable farming practices: soil degradation, declining water quality and disease outbreaks often lead to the abandonment of ponds after just a few production cycles, intensifying the pressure on remaining natural habitats as new areas are cleared. These dynamics highlight the urgent need for sustainable coastal management and the development of aquaculture systems that coexist with, rather than replace, mangrove ecosystems. Integrated mangrove-aquaculture systems, for example, offer a promising alternative that supports both environmental conservation and economic livelihoods (Ahmed et al., 2023; McSherry et al., 2023).

1.2. State of the art: earth observation data and methods for aquaculture inventory

Recent advances in Earth observation have enabled increasingly accurate assessments of mangrove extent, status, and change (Bunting et al., 2018, 2022; Du et al., 2023; Goldberg et al., 2020; Thomas et al., 2017). Early global efforts include the World Mangrove Atlas (1997), which compiled thematic maps, literature, and remote sensing data (Spalding et al., 2010). Giri et al. (2011) produced the first consistent global baseline using ~1000 Landsat scenes using hybrid classification methods. More recently, a 10-m resolution high-resolution global mangrove dataset was generated from Sentinel-2 imagery using object-based and random forest methods, providing a global mangrove extent map for 2020 (Jia et al., 2023). Complementing optical approaches, Thomas et al. (2017) used JERS-1 and ALOS PALSAR synthetic aperture radar (SAR) data to map global changes and identify land use drivers of mangrove loss. Goldberg et al. (2020) applied an NDVI anomaly algorithm and machine learning to the Landsat archive to detect temporal changes in mangrove and attribute losses to land-use categories. Building on these foundations, the Global Mangrove Watch (GMW) initiative (Bunting et al., 2022) delivered the most comprehensive long-term global mangrove extent dataset using a L-band SAR time series (JERS-1, ALOS, and ALOS-2), establishing radar-based monitoring as a robust method for mangrove mapping.

2. Materials and methods

2.1. Data

2.1.1. Aquaculture pond time series data

The aquaculture pond time series dataset is based on the comprehensive reference dataset of Asian coastal aquaculture ponds developed by Ottinger et al. (2026, 2022). An automatic, multi-sensor, object--based approach was used to extract and map individual pond aquaculture features at a single-object level for the year 2019 from Sentinel-1 and Sentinel-2 imagery (see Fig. 1). Both sensors are part of the Copernicus Earth Observation Program, which is operated by the European Space Agency (ESA). The mapping was refined using a Digital Elevation Model to retain only flat, low-lying coastal areas, and further filtered by shape and size to exclude unrelated water bodies. This resulted in the first continental-scale dataset of its kind, comprising 3.6 million ponds across 22 Asian countries, with an overall mapping accuracy of 91.9 percent. The dataset represents both freshwater and brackish water pond systems. To extend the reference dataset into a temporal analysis, annual water masks for 1984–2019 were generated using the multispectral Landsat archive. Landsat Surface Reflectance (SR) products, accessed via the Google Earth Engine in an analysis-ready format, provided consistent and calibrated input data (Gorelick et al., 2017). Temporal compositing, including median aggregation of multiple scenes, was employed to mitigate data gaps, seasonal variability, and technical issues such as Landsat 7's scan line failure, ensuring robust annual coverage. With more than 250 images for most land areas, the water status of each mapped pond could be reliably monitored. Linking the 2019 reference pond objects to these annual water masks captures the spatial and temporal evolution of aquaculture ponds along the Asian coast. The resulting pond dynamics dataset published by Ottinger et al. (2026) enables detailed analyses at national and district levels and provides insights into the long-term aquaculture development across 22 countries.

2.1.2. Mangrove extent data

The Global Mangrove Watch (GMW) dataset is a consistent, global time series of mangrove extent derived from Synthetic Aperture Radar (JERS-1 SAR, ALOS PALSAR, and Sentinel-1) and optical imagery. Owing to the discontinuous availability of L-band SAR missions underpinning the dataset (Ottinger and Kuenzer, 2020), mangrove extent is mapped for selected years rather than as a continuous annual record. The dataset has a spatial resolution of 25 m and covers the years 1996, 2007–2010, and 2015–2020 and is widely used to assess deforestation, restoration, and conservation outcomes in mangrove ecosystems. For this study, we used version 3 of the GMW dataset, which was downloaded from Zenodo (Bunting et al., 2022), to ensure reproducibility and alignment with the latest publicly available release. To maintain consistency with the temporal coverage of the pond dynamics reference dataset (1984–2019), only the corresponding GMW years up to 2019 were included in the analysis, while the 2020 GMW layer was intentionally excluded.

2.1.3. Administrative data

The Database of Global Administrative Areas (GADM, 2012) dataset was used as a reference for delineating pond aquaculture data at the national scale. While the pond dataset already included country affiliation as an attribute (see Ottinger et al., 2026), GADM additionally supported the analysis of mangrove loss by enabling the spatial intersection of the Global Mangrove Watch (GMW) data with country-level boundaries, ensuring precise attribution of mangrove changes to individual countries.

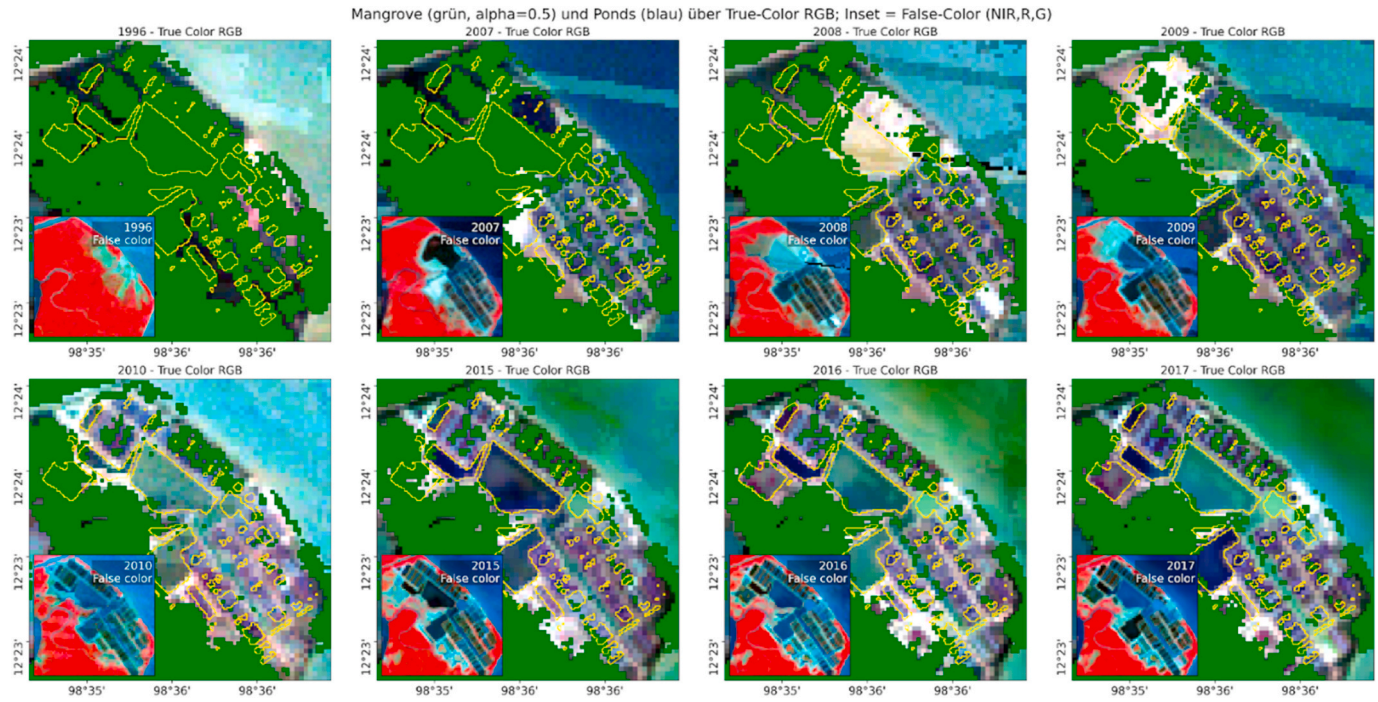


Fig. 1. Landsat median composite time series visualising the 2019 aquaculture pond reference dataset (Ottinger et al., 2026) alongside the annual mangrove extent for all years available from the Global Mangrove Watch dataset (Bunting et al., 2022): true-color RGB imagery with mangrove extent (green) and aquaculture pond boundaries (yellow), including false-color (NIR–red–green) insets. (For interpretation of the references to color in this figure legend, the reader is referred to the Web version of this article.)

2.2. Analysis of the relationship between Mangrove forests and aquaculture ponds

This part of the study examines the spatial and temporal interactions between aquaculture ponds and mangrove forests by systematically overlaying and comparing their datasets at the national level. The spatial analyses identifies areas where aquaculture ponds overlap with or replace mangroves, thereby quantifying the geographic extent of direct conversion. The temporal analysis tracks how these overlaps evolve over time, revealing sequences of mangrove clearance, pond construction, and commencement of aquaculture activities. Aligning the aquaculture dynamics dataset with the Global Mangrove Watch dataset, the analysis reveals patterns of mangrove loss associated with pond activation and highlights differences in the pace and intensity of these changes across Asian countries. To quantify mangrove dynamics, we analyzed the spatial intersections of consecutive time periods from 1996 to 2019 (e.g., 1996–2007, 2007–2008). Resulting polygons were classified into three categories: ‘Gain’ (new mangrove establishment), 'Loss' (disappearance of mangrove cover), and ‘Stable’ (persistence across both time steps). This classification formed the basis for calculating national level area changes.

2.2.1. Pond data initialization

First, the aquaculture pond polygons were imported and structured into a spatially referenced vector dataset with a metric projection. This allows accurate spatial calculations, such as measuring the area, to be performed. Each pond polygon contains attributes describing its year of activation. While a pond may be recorded as having been activated in a specific year, this process is gradual. First, the mangroves are cleared, then the dam is constructed, and only later does the site appear as a body of water in the dataset. To maintain consistency, a unique ID column is added to preserve feature references during spatial joins and intersections.

2.2.2. Intersection of aquaculture ponds and mangroves

The Global Mangrove Watch dataset provides snapshots of the mangrove extent for the selected years (1996, 2007–2010, 2015–2019) (Bunting et al., 2022b). Despite the discontinuous nature of the temporal coverage, it remains the most comprehensive dataset for large-scale mangrove monitoring. For each year, the mangrove polygons are reprojected and intersected with the pond polygons. The resulting attributes capture the mangrove area inside each pond. A threshold-based criterion is then applied: if mangroves cover more than 50% of a pond's area, the pond is flagged as containing “significant mangrove extent.” This threshold reduces errors resulting from differences in dataset resolution and boundary mismatches. Binary indicators (1 = >50% mangrove coverage, 0 = <50%) are stored as new columns for each year (e.g., m1996, m2007).

2.2.3. Temporal analysis of pond activation and Mangrove disappearance

In order to systematically assess the temporal relationship between aquaculture development and mangrove loss, we developed a harmonized time-indexing framework that integrates Landsat-based pond activation timelines with Global Mangrove Watch (GMW) presence/absence data. The framework is based on a year-by-year comparison of pond activation and mapped mangrove extent (see Fig. 2). As the GMW dataset is only available for selected years (1996, 2007-2010 and 2015–2020), substantial temporal gaps exist (1996–2007 and 2010–2015). To maintain analytical consistency across these uneven intervals, we replaced calendar years with a relative position index that aligns the continuous Landsat time series with the discrete GMW observation years (e.g., 1996 = 0, 2007 = 1). This approach prevents analytical distortions that would arise if irregular observation intervals were treated as evenly spaced, which could otherwise bias causal attribution.

For each pond polygon, we derived two key temporal attributes: the activation position, indicating when a pond first became operational (active), and disappearance position, marking the first GMW observation year at which mangrove cover within the pond boundary declined

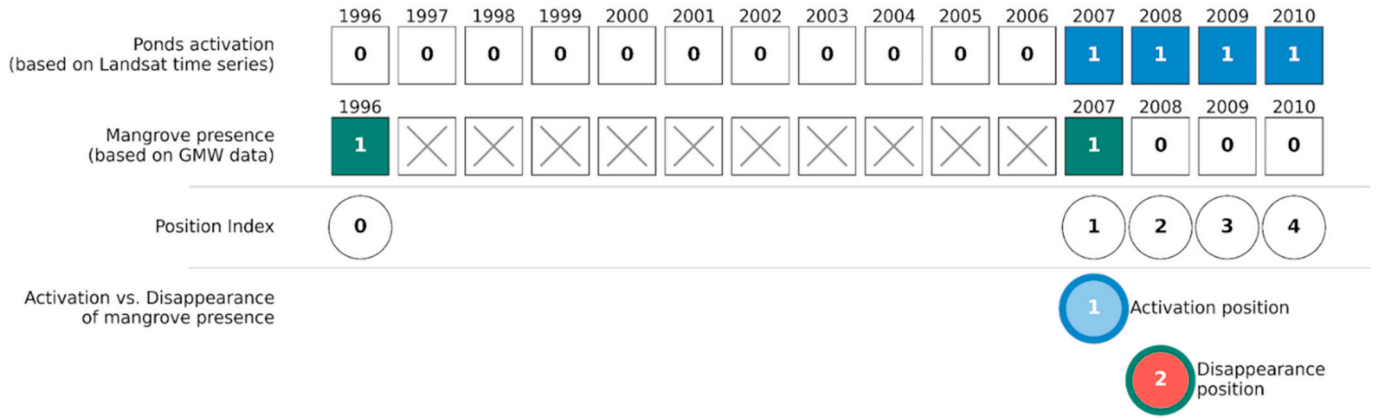


Fig. 2. Visualization of pond activation and mangrove presence dynamics over an exemplary period (1996–2010). The "activation position" (blue circle) marks the year mangroves first appear, while the "disappearance position" (red circle) marks when mangrove coverage ends. Blue and green boxes indicate pond activity and mangrove coverage, respectively. (For interpretation of the references to color in this figure legend, the reader is referred to the Web version of this article.)

by more than 50% relative to the pond area. Pond activation was obtained from Landsat time-series classifications following Ottinger et al. (2026), where aquaculture ponds receive a binary activation state (1 = active, 0 = inactive), while mangrove presence was extracted from the GMW data. Using positional indices ensures consistent temporal alignment between these heterogeneous datasets and reduces misclassification risks associated with irregular observation intervals, providing a coherent temporal framework for reliably identifying causal relationships between pond activation and subsequent mangrove decline. We then quantified mangrove area directly lost as a consequence of aquaculture pond construction or activation by calculating changes in mangrove extent within each pond between the position immediately preceding activation and the disappearance position. This method captures both immediate effects of pond activation and earlier reductions related to construction activities or ongoing maintenance. The resulting mangrove loss per pond was stored as a new attribute in square meters. Fig. 2 illustrates the temporal dynamics of pond activations and mangrove presence over an example period (1996 – 2010). Pond activity derived from Landsat and mangrove presence from GMW are aligned using the position index to identify key transition events. A conservative causality criterion was applied, whereby mangrove loss was attributed to pond activation only if it occurred within two consecutive observation positions after activation. This threshold, adjustable by expert judgement, identifies cases of direct conversion while minimizing false associations due to unrelated environmental changes. To avoid confounding effects from intermittent pond use or mangrove regrowth, only the first instance of mangrove loss per pond was considered.

2.2.4. *Quantification of Mangrove area lost to aquaculture ponds*

To determine whether aquaculture pond activation directly causes mangrove loss, we applied a time-based rule using the positional index timeline. Mangrove loss is only considered causally linked if it occurs at the same observation step as pond activation or within the next two steps, corresponding to a positional index difference of 0 to 2 (see Fig. 3).

The positional index timeline rule excludes cases where mangrove loss occurred before pond activation, avoiding incorrect causal links.

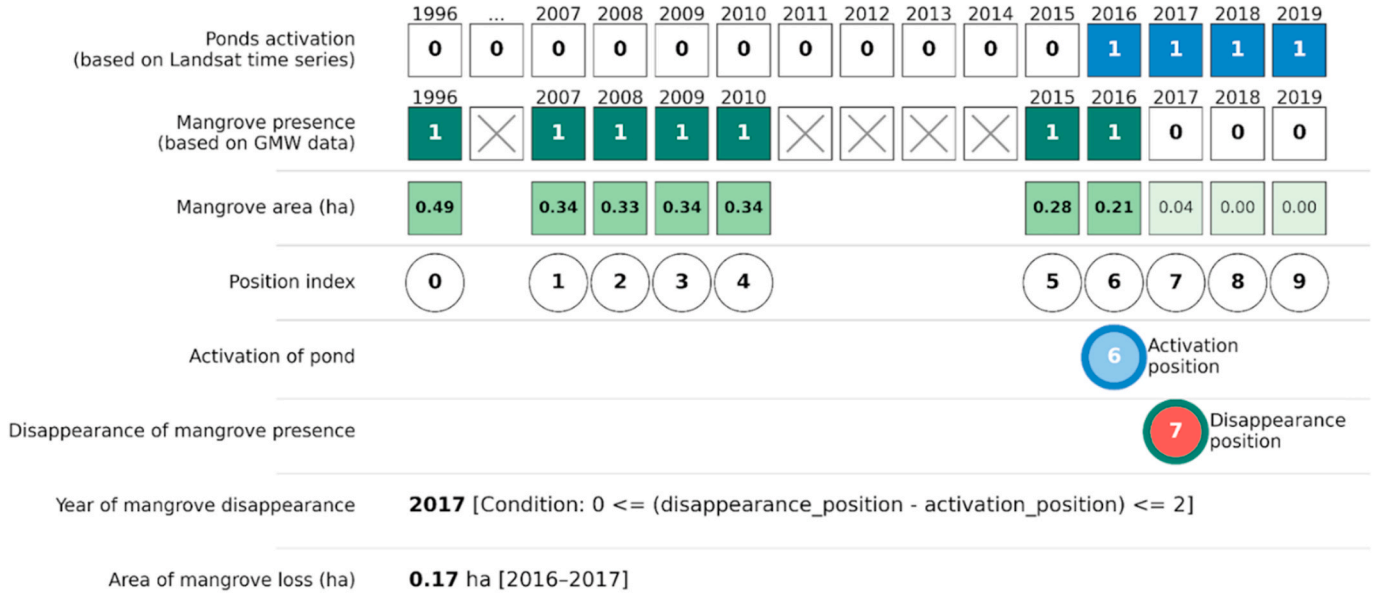


Fig. 3. Detailed dynamics for a single aquaculture pond from 1996 to 2019. Light green boxes illustrate the mangrove area (ha) within the pond polygon. Pond activation occurs at position 6 (2016), the first active year. Mangrove disappearance at position 7 (2017) is defined as mangrove cover dropping below 50% of the pond area. According to the association rule, mangrove loss is linked to pond activation if disappearance follows within two years, assigning loss to 2017. The mangrove loss area between 2016 and 2017 is 0.17 ha. (For interpretation of the references to color in this figure legend, the reader is referred to the Web version of this article.)

Once the positional index of disappearance is identified, it is translated into the corresponding calendar year using the observation timeline. The processing workflow first checks whether a pond has a recorded activation position. It then verifies that mangrove disappearance is observed and occurs no later than two observation periods after activation.

If these conditions are met, the year of mangrove disappearance is stored in a new dataset column; otherwise, the value is set to null (no data). This approach allows for short ecological response delays while maintaining temporal consistency in linking pond establishment to mangrove loss. It captures preparatory impacts, such as mangrove clearing and land modification during pond construction. The resulting dataset provides a spatially explicit, pond-level quantification of mangrove loss, enabling aggregation at national and regional scales. By linking pond activation timing with subsequent mangrove decline, this methodology enables a robust assessment of the direct impact of aquaculture expansion on coastal forests.

3. Results

3.1. Mangrove forest area in Asia

The spatial analysis shows a clear concentration of mangrove resources in Asia, accounting for over one-third (39.1%) of the global mangrove extent, with Indonesia contributing nearly one-fifth worldwide. As shown in Fig. 4, Indonesia clearly emerges as the country with the largest mangrove area by a wide margin. In 2020, almost half (49.2%; 29365 km^2) of the mangroves in our study region, Asia, were located in Indonesia. More broadly, Asia contains over one-third (39.1%) of the world's total mangrove area, with Indonesia alone accounting for nearly one-fifth (19.9%) of the global mangrove coverage. Bangladesh, Myanmar, and Malaysia follow Indonesia, though with substantially smaller extents. Together, these countries represent a significant portion of Asia's total mangrove forests, emphasizing Indonesia's predominant role in the regional mangrove landscape.

We then produced a series of graphs to illustrate how mangrove extent has changed over time: Fig. 5 presents temporal trends in mangrove extent from 1996 to 2019 for all relevant coastal countries in Asia. The data indicate a consistent decline in mangrove area across most countries during the late 1990s and early 2000s. Indonesia experienced the largest absolute loss, with mangrove area decreasing by approximately 7.2% (2.284 km^2) between 1996 and 2020. Despite this drop, Indonesia still has the largest total mangrove area by far. Similar, though smaller, losses occurred in Myanmar (8.9%, 564 km^2) and Pakistan (22.2%, 269 km^2), reflected in the downward slopes of the mangrove extent curves during this period. Steep relative declines can be observed in Sri Lanka and Iran, losing nearly 30% (~80 km^2) and 28% (~50 km^2) of their mangrove areas respectively, indicating substantial degradation or conversion of mangrove habitats in these countries over the period. India, Malaysia, Philippines, Thailand, and Vietnam all experienced moderate losses ranging from roughly 1.7% to 6%, underscoring ongoing pressures on mangroves across South and Southeast Asia. While Fig. 5 presents coverage data for all 18 coastal Asian countries, subsequent analyses focus on the 12 most important Asian coastal countries in terms of mangrove extent and loss, excluding very small countries such as Brunei, East Timor, and Singapore for clarity and relevance.

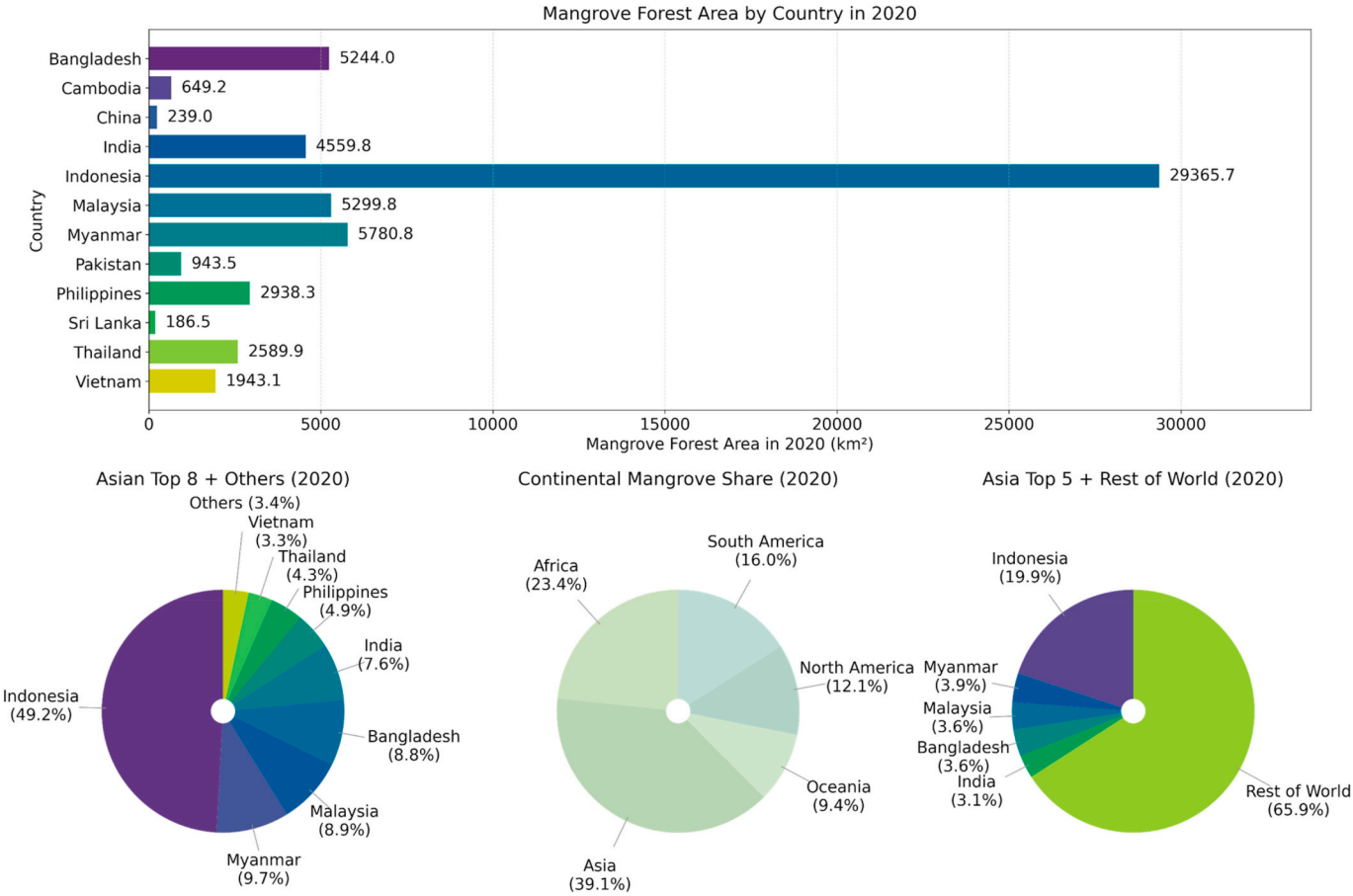


Fig. 4. Top: Mangrove forest area in 2020, focused on Asia' top mangrove-holding nations. Bottom: Continental and regional distribution of global mangrove area, Source GMW (Bunting et al., 2022b).

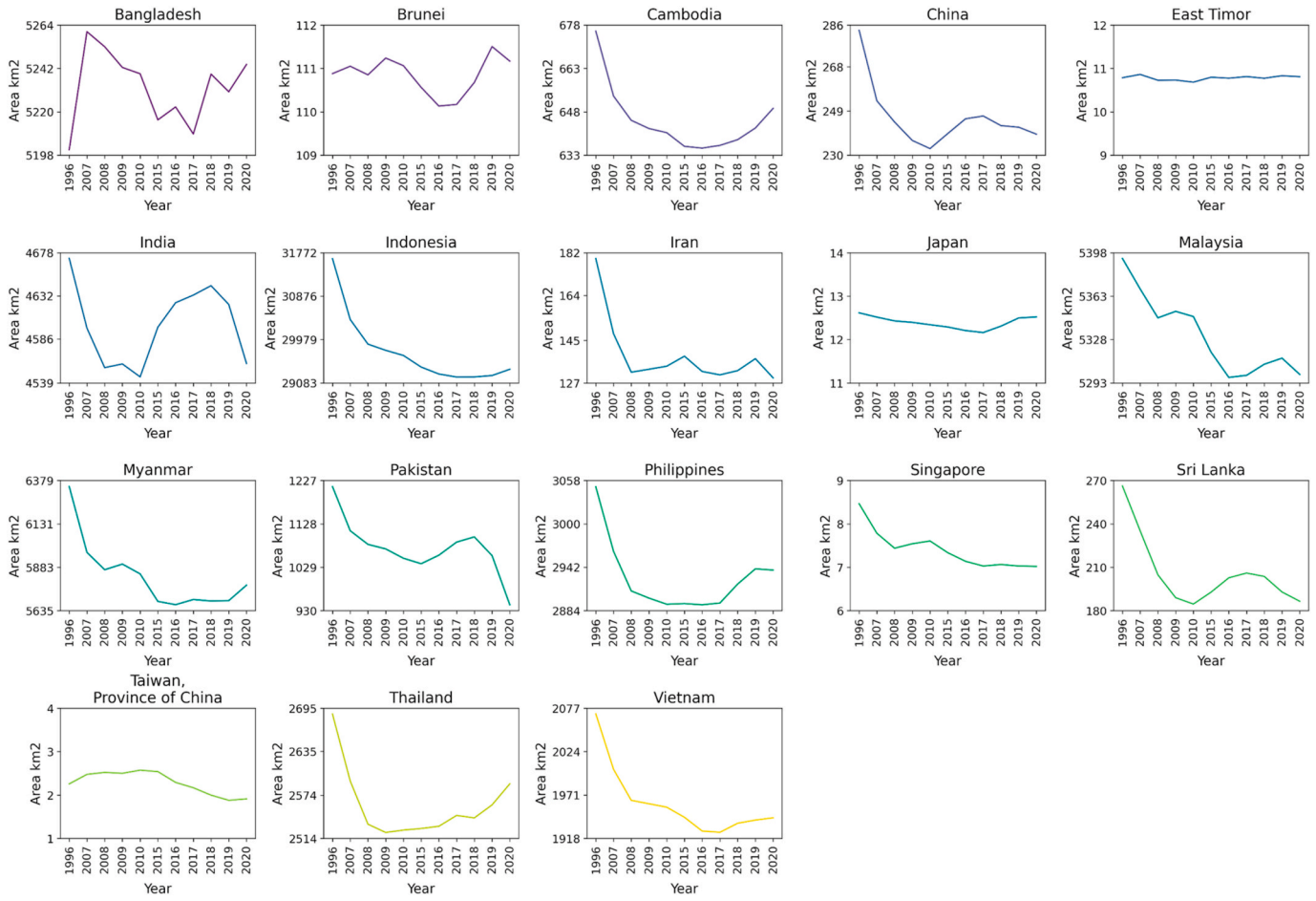


Fig. 5. Temporal trends in mangrove extent across coastal Asian countries, illustrating changes in mangrove cover over time. The line plots depict mangrove area (km^2) across time intervals aligned with Global Mangrove Watch (GMW) data availability, highlighting both increases and decreases in mangrove extent by country.

3.2. Analysis of Mangrove loss and Mangrove gain

Evaluating the balance between mangrove expansion ('Gain') and deforestation ('Loss') provides a nuanced view of regional ecosystem dynamics. The analysis highlights that while mangrove regeneration occurred throughout the study period, it was historically outweighed by massive deforestation events, particularly in the earlier observation phases. Fig. 6 reveals substantial differences in mangrove losses between year-pair intervals of varying lengths. The largest decline is observed between 1996 and 2007, which spans 11 years, followed by the period between 2010 and 2015 with a four-year interval. Furthermore, the analysis highlights the 12 countries with the greatest losses in mangrove extent, identifying those nations in Asia that have experienced the most significant reductions over the study period.

3.3. Pond activation and Mangrove loss

At the local level, the interaction between aquaculture ponds and the surrounding mangrove ecosystems is particularly evident when the spatial and temporal development of individual pond clusters is examined. At a representative coastal site in the Andaman Sea in Myanmar, for example, aquaculture ponds are embedded within an area that was originally part of a continuous mangrove landscape (see Fig. 7). This allows us to assess in detail how the pond activation and expansion has influenced mangrove persistence over a period of more than two decades. The spatial arrangement of these ponds enables us to analyse their operational history and the corresponding ecological consequences. The temporal matrices in Fig. 7 (see B and C) illustrate two complementary dimensions: the activation status of each pond across time and the proportion of mangrove cover remaining within the pond boundaries during the same years. When these layers are evaluated in combination, a clear alignment emerges: periods in which the reference ponds (pond polygons were identified in 2019) transition into active state correspond with marked reductions in mangrove extent within their boundaries. This synchronicity illustrates the direct impact of pond activity on mangrove ecosystems as a principal driver of localised mangrove loss. Notably, the bottom rows in Fig. 7 reveal that reductions in mangrove extent correspond with changes visible in the false-color annual median images time series. This alignment provides strong satellite-based evidence supporting the observed mangrove loss associated with aquaculture activities. For example, pond number 1-5 clearly shows a sustained decline in mangrove coverage since 1996, consistent across both mangrove maps and satellite imagery.

At the regional level, the spatial footprint of aquaculture-driven mangrove degradation reveals broader patterns beyond the individual case study. Mapping all ponds associated with mangrove disappearance across the study area (see Fig. 8) highlights distinct clusters, particularly concentrated in Indonesia and, to a lesser extent, Myanmar and Vietnam. These clusters represent locations where aquaculture development has expanded rapidly, resulting in significant ecosystem conversion. Histograms aggregated by latitude and longitude underscore these spatial concentrations and reveal the strong geographic variation in the impacts of aquaculture.

Temporal analysis across all ponds suggests that mangrove loss may have been uneven throughout the study period, potentially occurring in distinct phases of intensified activity. Notably, more pronounced losses

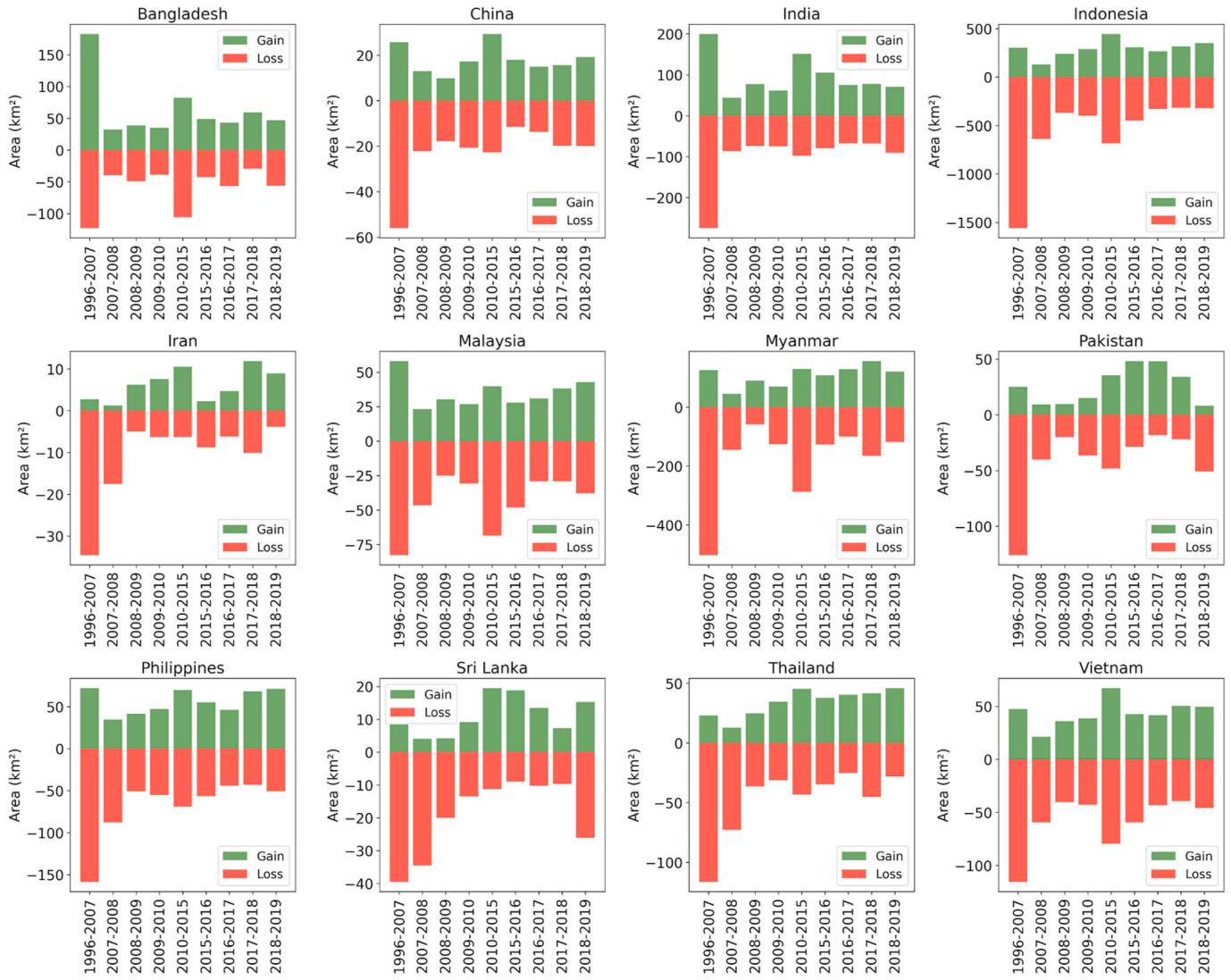


Fig. 6. Mangrove area gains (green) and losses (red) from 1996 to 2019 for 12 selected Asian coastal countries, shown as bar charts for specified time intervals corresponding to Global Mangrove Watch (GMW) data availability. (For interpretation of the references to color in this figure legend, the reader is referred to the Web version of this article.)

appear to have taken place during 1996–2007, 2007–2008, and 2008–2009, which could indicate waves of pond establishment. These temporal clusters likely reflect cyclical or policy-driven dynamics within the aquaculture sector, although further investigation is needed to confirm such drivers.

3.4. Mangrove loss on aquaculture ponds

Comparing the temporal trajectories of total mangrove loss with aquaculture-specific loss (see Fig. 9) reveals distinct national phases of pressure on mangrove ecosystems. In Thailand and Vietnam, these two variables closely follow each other during early periods of aquaculture expansion, suggesting a strong link between aquaculture growth and mangrove decline. In contrast, China shows a notable divergence between the trends, indicating other factors may also be influencing mangrove loss. These patterns provide insight into how the relationship between aquaculture development and mangrove degradation varies across countries in the study region, reflecting differing local contexts and pressures.

Fig. 10 displays total mangrove area losses (green line) alongside mangrove losses specifically due to aquaculture expansion (blue line). The results highlight periods during which aquaculture appears to have exerted greater pressure on mangrove ecosystems. However, it is important to acknowledge the limitations of the data, particularly the temporal gaps between 1996–2007 and 2010–2015, for which only cumulative net changes are available. While overall losses can be identified during these intervals, the exact timing and progression within these years remains unclear, meaning short-term trends should be interpreted with caution. Nevertheless, the cumulative data over the full study period provide robust insights into long-term trends and form the basis for the subsequent analysis.

There is a strong positive relationship between aquaculture expansion and overall mangrove decline across most studied nations. To quantify this relationship, we calculated Pearson's correlation coefficient between aquaculture pond density and total mangrove loss density (both normalized by municipality area) across GADM level 2 municipalities within each country (Table 1, Fig. 10). Correlations were positive and statistically significant in all countries examined individually (Pearson's $r = 0.34–0.90$; $R^2 = 0.12–0.81$; $p < 0.05$ in all cases; $n = 39–746$ municipality-year observations per country), and remained significant when pooled across all 12 countries ($r = 0.77$, $R^2 = 0.6$, $p < 0.001$). This linearity indicates that in countries with high total mangrove loss, aquaculture is consistently a primary or proportional driver of that degradation. The strongest correlations were observed in

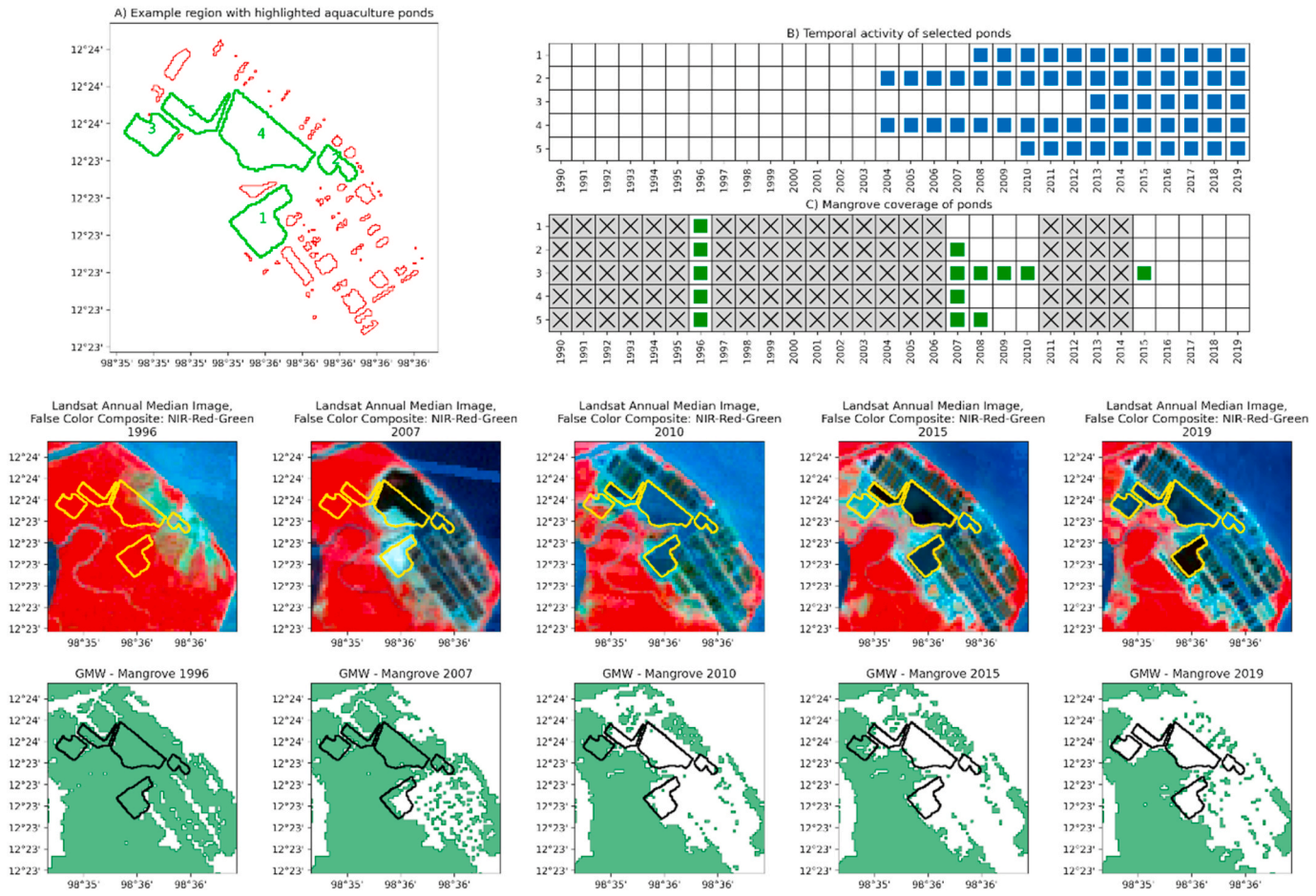


Fig. 7. Spatial distribution and temporal dynamics of selected aquaculture ponds and adjacent mangrove coverage. The top-left map (A) locates the ponds, while the two matrices (B, C) illustrate pond activity and mangrove presence over time. The bottom rows show corresponding satellite imagery and GMW data across selected years.

Vietnam, Myanmar, Sri Lanka, Cambodia, and China (r = 0.82–0.90), consistent with aquaculture being a major driver of mangrove degradation in these countries. Pakistan is an unusual case in that mangrove loss due to aquaculture nearly disappeared after 2007 (see Fig. 9), only to re-emerge slightly in the final year of the analysis. This pattern warrants further investigation to understand the underlying causes.

The spatial distribution of aquaculture ponds and mangrove ecosystems across Asia reveals distinct geographic patterns and clear interactions between aquaculture development and coastal habitats (see Fig. 10). Aquaculture ponds are strongly clustered in major coastal river deltas, where pond area is particularly concentrated, indicating regions of intensive aquaculture activity (Fig. 10A). In contrast, mangrove cover in 2019 remains most extensive in Bangladesh, Myanmar, Thailand (including the Gulf of Thailand), and parts of Indonesia, notably Southeast Sumatra, East Borneo, and Sulawesi (Fig. 10B). These remaining mangrove regions are often spatially separated from the most densely developed pond clusters. The spatial pattern of total mangrove loss between 1996 and 2019 reveals distinct degradation hotspots that frequently coincide with areas of high aquaculture pond density (Fig. 10C). This overlap becomes even more apparent when focusing on ponds directly associated with mangrove loss (Fig. 10D), which are concentrated in regions experiencing the most severe declines in mangrove extent. Particularly in Indonesia and Myanmar, the close spatial correlation between pond expansion and mangrove loss indicates that aquaculture development has been a dominant driver of mangrove degradation. Together, the heatmaps emphasize a strong spatial overlap between pond expansion and mangrove loss, underscoring the substantial environmental footprint of pond aquaculture on coastal ecosystems in Asia.

Fig. 11 further illustrates these dynamics across four major mangrove conversion hotspots: Northwest Myanmar, East Borneo, Southeast Sumatra, and Central Sulawesi. Across all regions, areas with the highest mangrove loss attributed to pond activation (Fig. 11 A1–D1) consistently coincide with zones of dense pond coverage in 2019 (Fig. 11 A2–A3, B2–B3, C2–C3, D2–D3). This pattern is particularly pronounced in Indonesia, where extensive pond aquaculture systems have replaced formerly contiguous mangrove landscapes. The distribution of remaining mangroves in 2019 (Fig. 11 A4–D4) shows increasing fragmentation around aquaculture clusters, reflecting the long-term structural changes in coastal ecosystems. Overall, these spatial patterns demonstrate that historical mangrove loss and present-day aquaculture intensity are closely aligned, emphasizing the central role of pond expansion in reshaping Asia's coastal zones. According to our analysis, the contribution of aquaculture-related activities to mangrove loss varies significantly across countries and time periods. By contextualizing aquaculture-driven loss within total mangrove decline, Fig. 12 illustrates these differences in proportional impact. While it represents a smaller proportion of total mangrove loss compared to other drivers, Indonesia, Vietnam, and Myanmar consistently exhibit the highest shares attributable to aquaculture. This highlights the sustained and pronounced pressure aquaculture exerts on mangrove ecosystems in these regions, marking them as key hotspots of aquaculture-driven degradation.

To further examine these dynamics, we analyzed the temporal co-

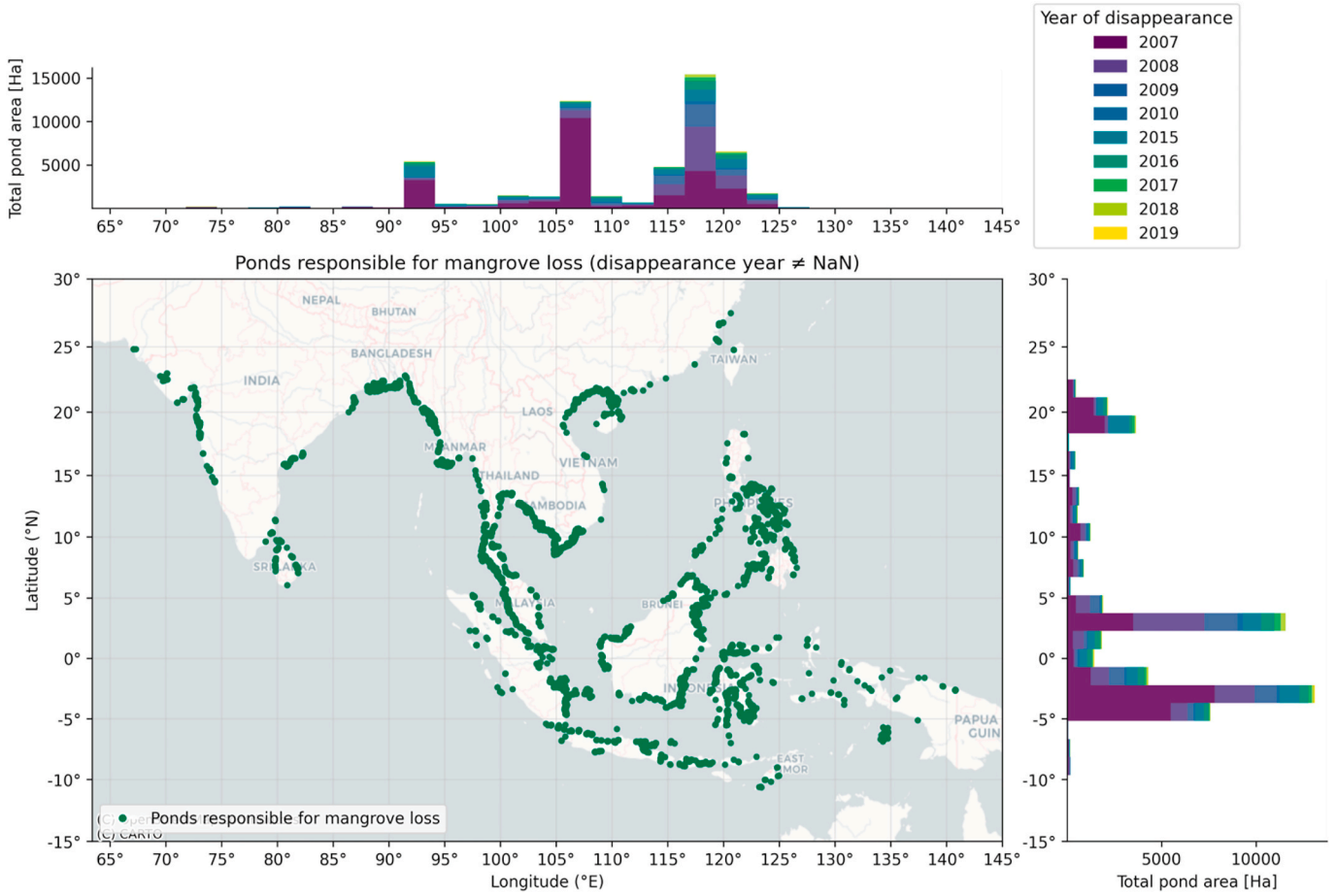


Fig. 8. Spatial distribution of ponds causing mangrove loss, colored by disappearance year. Histograms show pond area aggregated by longitude (top) and latitude (right), revealing spatial and temporal patterns of mangrove degradation.

occurrence of pond activity and mangrove presence across 12 countries (Fig. 13). Paired subplots illustrate mangrove loss due to pond activation (left, teal bars), calculated as the change in mangrove area from the last year without pond activity to the year of disappearance, alongside total mangrove area over time within affected ponds (right, green bars), capturing broader trends in mangrove extent within aquaculture areas (see Fig. 14).

Indonesia stands out as having suffered the highest cumulative loss, at 13,045.8 ha between 1996 and 2007 – over ten times greater than any other country. Although losses decline afterward, they remain substantial, including 5284.8 ha (2007–2008), 2718.2 ha (2008–2009), and 2177.6 ha (2010–2015), followed by continued activity in later periods (497.8 ha in 2016–2017; 348.3 ha in 2017–2018; 52.2 ha in 2018–2019). Myanmar is the second major hotspot, with 2891.5 ha lost in 1996–2007, a decline to 150.3 ha and 36.0 ha in the next two intervals, and a renewed peak of 1000.9 ha in 2010–2015. Subsequent years still show notable losses, including 204.9 ha (2015–2016) and 108.1 ha (2016–2017). Countries with intermediate losses (i.e. Thailand, Malaysia, the Philippines, Vietnam, India, and China) show similar trajectories characterized by an early peak followed by pronounced declines. For example, losses in Thailand decreased from 213.5 ha to consistently below 60 ha after 2010, while Vietnam declined from 459.1 ha to below 40 ha after 2015. The Philippines decrease from 184.4 ha to just 4.4 ha by 2018–2019. India records 307.6 ha early on but stabilizes at low levels (<53 ha per period). In contrast, Bangladesh, Sri Lanka, and Cambodia experienced minimal losses throughout the study period.

Overall, mangrove loss peaked strongly between 1996 and 2007 across all countries before declining sharply, although Indonesia and Myanmar continued to exhibit elevated losses later in the time series. These patterns underscore the uneven spatial and temporal distribution of mangrove conversion, reflecting differences in national aquaculture development and coastal land-use trajectories.

4. Discussion

4.1. Methodological strengths & relevance

This study demonstrates an effective approach for integrating heterogeneous Earth observation datasets with contrasting temporal resolutions to analyse interactions between aquaculture expansion and mangrove loss. By harmonizing irregular mangrove observation years with annually resolved Landsat-based pond activation data, the analysis enables consistent cross-dataset comparison despite substantial differences in temporal sampling. This is particularly important for long-term coastal monitoring, where uneven data availability can obscure cause–effect relationships. A key strength of the approach lies in its ability to assess temporal ordering, allowing mangrove loss to be linked to aquaculture pond activation rather than coincidental change. Emphasizing first-occurrence events of pond activation and mangrove disappearance reduces confounding effects from intermittent pond use, abandonment, or mangrove regrowth, which are common in coastal aquaculture landscapes. The object-based linkage of aquaculture pond geometries with mangrove extent data enables spatially explicit, pond-level attribution of mangrove loss across multiple countries. This moves beyond aggregated assessments and offers information that is directly relevant for coastal spatial planning and management. The combined visualization of pond activity and mangrove presence further

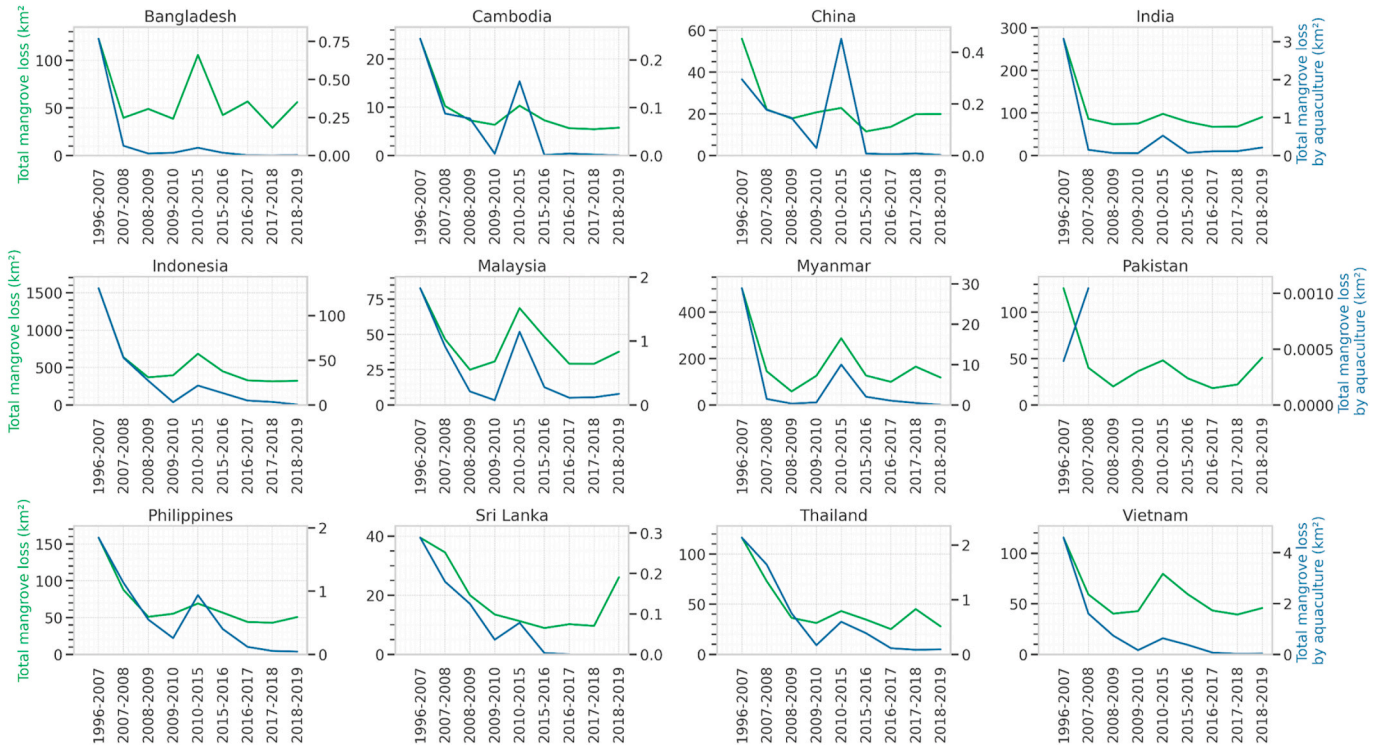


Fig. 9. Temporal trends in total mangrove loss (green line, left axis) and mangrove loss attributable to aquaculture pond expansion (blue line, right axis) for twelve Asian coastal countries between 1996 and 2019. Time intervals correspond to Global Mangrove Watch (GMW) data availability and are of unequal length (e.g., 11 years for 1996–2007, 1 year for most intervals from 2015 onward); values for the 1996–2007 and 2010–2015 intervals represent cumulative net change over the full interval rather than annual rates. Note the differing y-axis scales across countries and between the two loss measures within each panel. (For interpretation of the references to color in this figure legend, the reader is referred to the Web version of this article.)

enhances interpretability and supports communication of complex spatio-temporal dynamics to non-specialist audiences. Such clarity is indispensable in interdisciplinary contexts where ecological, hydrological, and socio-economic factors converge.

4.2. Limitations

Several limitations should be considered when interpreting the results. First, the reliance on discrete GMW observation years restricts mangrove monitoring to relatively coarse temporal intervals, potentially overlooking short-term or rapid mangrove changes occurring between observation dates. Mangrove extent data from the Global Mangrove Watch are available only for selected years, limiting temporal precision during extended gaps such as 1996–2007 and 2010–2015. While the positional index harmonizes timelines of the pond and mangrove datasets for comparative analysis, it cannot fully substitute for the temporal resolution needed to capture finer-scale dynamics within these gaps. As a result, the effective calendar-time tolerance of our causal-attribution rule is not constant: it is one year during densely observed periods but extends to several years within the two gap intervals. Loss attributed to pond activation during 1996–2007 and 2010–2015 should therefore be interpreted with more caution than loss attributed in years with near-annual GMW coverage, as totals for these intervals may include an unknown proportion of mangrove loss not directly caused by the associated pond activation.

Second, the focus on first-event detection excludes subsequent processes such as mangrove recovery, repeated clearance, or cyclical pond use. While ecologically relevant, these dynamics fall outside the scope of the present analysis. In addition, uncertainties inherent in remote sensing classification—stemming from both Landsat-based pond status (active/non-active) detection and GMW mangrove mapping—propagate through the analysis and may influence the precision of the results. Nevertheless, cumulative patterns over the full study period provide a robust basis for regional and national-scale interpretation.

Third, pond-level attribution is sensitive to the spatial resolution of the GMW dataset (25 × 25 m, 625 m^2), particularly for ponds near or below one pixel in area. Such ponds accounted for 49–62% of ponds classified as mangrove-covered, varying during the study period, indicating this affects a substantial portion of attributed loss. Across the 12 study countries, the share of all ponds classified as mangrove-covered (≥50% threshold) declined from 4.83% in 1996 to 2.59% in 2018 as the underlying pond distribution expanded, with 184,167 ponds (5.23% of the full pond dataset) classified as mangrove-covered in at least one study year (Supplementary Table 1). Comparing the distribution of computed mangrove-coverage fractions across five pond size classes (≤625 m^2, 625–1250 m^2, 1250–2500 m^2, 2500–10000 m^2, >10000 m^2; Supplementary Figs. 1–4), we found that the share of ponds classified as ≥90% mangrove-covered declined monotonically with increasing pond size (consistent across all study periods, see Supplementary Fig. 4).

One possible explanation is that smaller ponds more often result from clearing a small mangrove patch entirely, whereas larger ponds more often expand into adjacent non-mangrove land, which would lower their coverage fraction for real, biophysical reasons rather than a data-processing effect. However, this pattern is concentrated sharply in the ≥90% coverage bin rather than spread smoothly across intermediate coverage values (Supplementary Fig. 1 and Supplementary Fig. 2). This pattern is better explained by a mismatch between pond size and the 25m × 25m (625 m^2) mangrove pixel size (GMW data): a pond close to or smaller than one mangrove pixel often falls entirely within a single mapped mangrove cell, which pushes its calculated coverage toward 100% regardless of how much mangrove was actually present. A larger pond, spanning many pixels, produces a coverage value averaged across dozens of cells and so can land anywhere between 0% and 100%. We cannot fully rule out a contribution from genuine small-scale clearance

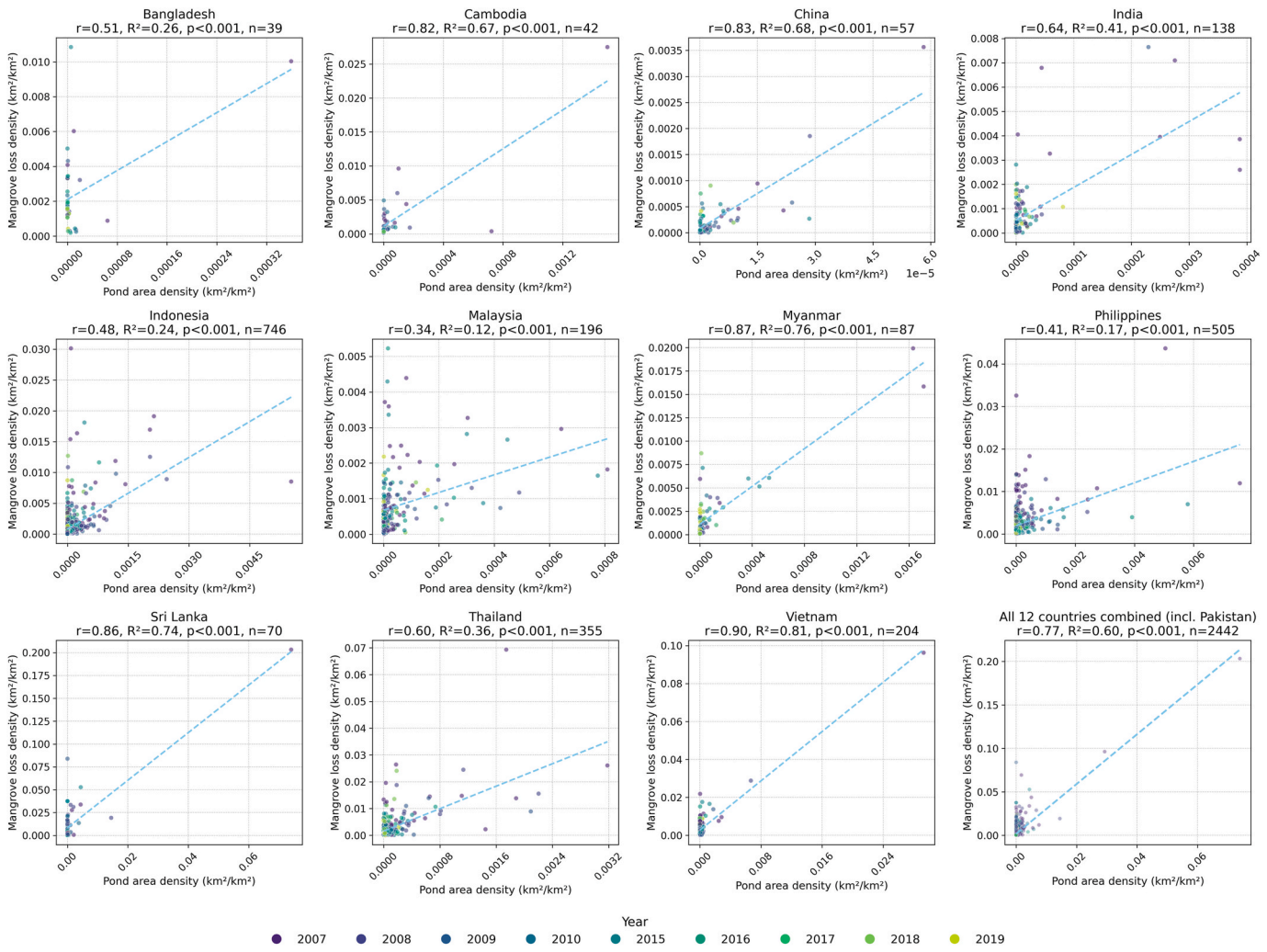


Fig. 10. Correlation between aquaculture pond density and mangrove loss density (both normalized by municipality area) across municipalities in eleven countries, plus a pooled panel for all twelve countries (bottom right, includes Pakistan). Points are colored by year of recorded mangrove loss; dashed lines show OLS regression fits. Pearson's r, R^2, p-value, and n are reported per panel. Pakistan was excluded from individual-country analysis due to insufficient sample size (n = 3).

Table 1
Correlation between aquaculture pond density and total mangrove loss density (both normalized by municipality area) across GADM level 2 municipalities, by country.

Country	n_obs[1]	n_muni[2]	Pearson's r	R^2
Bangladesh	39	10	0.51	0.26
Cambodia	42	13	0.82	0.67
China	57	14	0.83	0.68
India	138	34	0.64	0.41
Indonesia	746	165	0.48	0.24
Malaysia	196	46	0.34	0.12
Myanmar	87	13	0.87	0.76
Philippines	505	218	0.41	0.17
Sri Lanka	70	27	0.86	0.74
Thailand	355	73	0.60	0.36
Vietnam	204	47	0.90	0.81
all 12 (incl. Pakistan)	2442	662	0.77	0.6

[1] n_obs = municipality-year observations used in the correlation; [2] n_muni = distinct GADM level 2 municipalities represented. Pearson's r = strength/direction of the linear relationship (−1 to +1); R^2 = proportion of variance in mangrove loss density explained by pond density; All correlations were statistically significant at $p < 0.001$ (p-value = statistical significance of the correlation). Pakistan (n obs = 3) was excluded from individual-country analysis due to insufficient sample size for reliable correlation estimation.

patterns, but we note this as a direction for further investigation.

We further examined the share of ponds with coverage values close to our 50% classification threshold (40–60% band), restricted to ponds with detectable mangrove signal (>10% coverage); small ponds showed a lower share in this near-threshold band (7.4%) than mid-sized ponds (14.9–22.0%). We do not interpret this as evidence of greater reliability for small ponds - rather, it reflects the same scale mismatch described above: because smaller ponds span only 1–2 pixels, their coverage values are pushed toward the extremes (0% or 100%) rather than intermediate values, so classification errors for these ponds tend to manifest as confidently incorrect outcomes rather than close calls near the threshold.

Total mangrove area within ponds declined markedly in the higher coverage bins (50–75% and especially 75–100%) over the study period, with the largest declines concentrated in larger ponds >1 ha (Supplementary Figs. 3 and 4). The 0–25% bin increased slightly correspondingly over the same period, consistent with ponds transitioning into lower coverage classes as mangrove within their footprint is progressively cleared. This pattern indicates the size-related measurement limitation described above does not drive the overall temporal trend our analysis is based on, since the shift in coverage-bin composition reflects genuine mangrove loss rather than a size-driven classification artifact.

To directly test whether the limitation affects our core findings, we

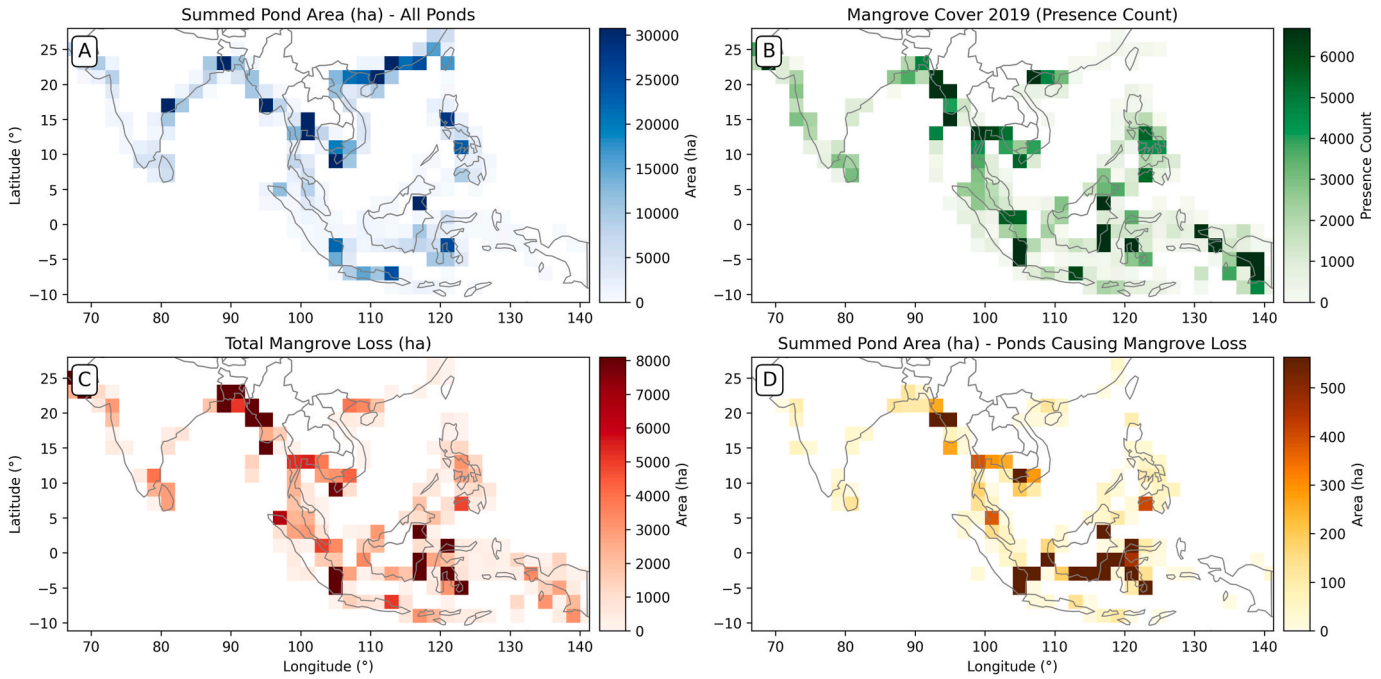


Fig. 11. Heatmaps showing total aquaculture pond area in 2019 (A), mangrove cover in 2019 based on GMW data (B), total mangrove loss from 1996 to 2019 (C), and pond areas linked to mangrove loss across Asia (D).

re-ran the correlation analysis in Table 1 excluding ponds at or below one GMW pixel (≤625 m^2; 2442 → 1975 municipality-year observations retained, 80.9%; Supplementary Table 2). Rather than weakening, the pooled correlation strengthened under this exclusion ($r = 0.83$, $R^2 = 0.69$, compared to $r = 0.77$, $R^2 = 0.60$ for the full dataset; Supplementary Fig. 5), with comparable or improved correlations in all countries except China, which declined marginally (0.83 → 0.82); Pakistan's sample was too small to interpret (n = 1). This pattern is consistent with attenuation bias: measurement noise from unreliable small-pond coverage estimates conservatively weakens the observed correlation, meaning our originally reported r = 0.77 likely represents a lower-bound estimate of the true underlying relationship between aquaculture pond density and mangrove loss. Future work using higher-resolution mangrove cover baseline data, or attribution methods that explicitly account for pond-to-pixel size ratios, would help improve coverage estimates for smaller ponds.

Finally, while aquaculture pond density showed a statistically significant positive correlation with total mangrove loss density across all countries analyzed (see Section 3.3), pond-attributed loss accounted for only a small proportion of total measured mangrove loss in most municipalities (median <1%). This reflects the strict design of our attribution rule rather than a limited role for aquaculture: loss is counted only when a pond crosses the 50% threshold, so ponds built on sites that were partly (but not predominantly) covered by mangrove are excluded, even though the mangrove present was cleared entirely. The reported share should therefore be read as a minimum estimate. Accordingly, the observed correlation reflects a broader spatial association between aquaculture presence and mangrove decline, rather than direct causal attribution of most loss events to pond construction itself. Other drivers not captured in the pond-level data, such as logging, agricultural conversion, or natural disturbance, likely account for the majority of measured mangrove loss even where aquaculture density is high.

4.3. Future directions for coastal earth observation

The temporal approach presented here is transferable to other coastal land-use interactions characterized by uneven observation frequencies, including urban expansion or wetland conversion. Future work could incorporate finer-scale, higher-frequency mangrove time series and automated change detection (e.g. event detection through machine learning or advanced pattern recognition algorithms) to better capture complex land-use trajectories.

Recent and upcoming Earth observation missions provide exciting opportunities to improve mangrove monitoring. In particular, active L-Band Synthetic Aperture Radar (SAR) sensors such as PALSAR-3 onboard ALOS-4, along with ongoing missions like NASA's NISAR and ESA's BIOMASS, offer consistent, long-term, all-weather capability to measure forest structure and biomass dynamics. These sensors enable more precise quantification of mangrove extent, canopy height, and carbon stocks, allowing detection of subtle degradation and recovery processes that are difficult to capture with optical or C-Band SAR data alone. Integrating these data with long-term optical time series will substantially enhance monitoring capacity and support near-operational assessments of coastal ecosystem change.

4.4. Implications for aquaculture-driven Mangrove change in Asia

The results show that aquaculture expansion has been a major, though spatially uneven, driver of mangrove loss across Asia. Indonesia emerges as the primary hotspot in terms of both total mangrove extent and absolute loss linked to aquaculture expansion (pond activation), followed by Myanmar and Vietnam. Spatial clustering of aquaculture ponds in low-lying coastal zones frequently coincides with historic mangrove decline, highlighting regions where mangrove ecosystem conversion has been most intense.

At the same time, weaker associations in some countries indicate that aquaculture is not the sole driver of mangrove loss and that national development pathways and management practices may play a critical role. By linking the timing of pond activation with subsequent mangrove disappearance, this study provides spatially explicit evidence to support integrated coastal management strategies that promote coexistence between aquaculture development and mangrove conservation. These findings underscore an urgent need for management approaches that foster sustainable aquaculture alongside mangrove conservation rather than replacement. The research advances understanding of the spatial and temporal patterns driving aquaculture-related mangrove loss,

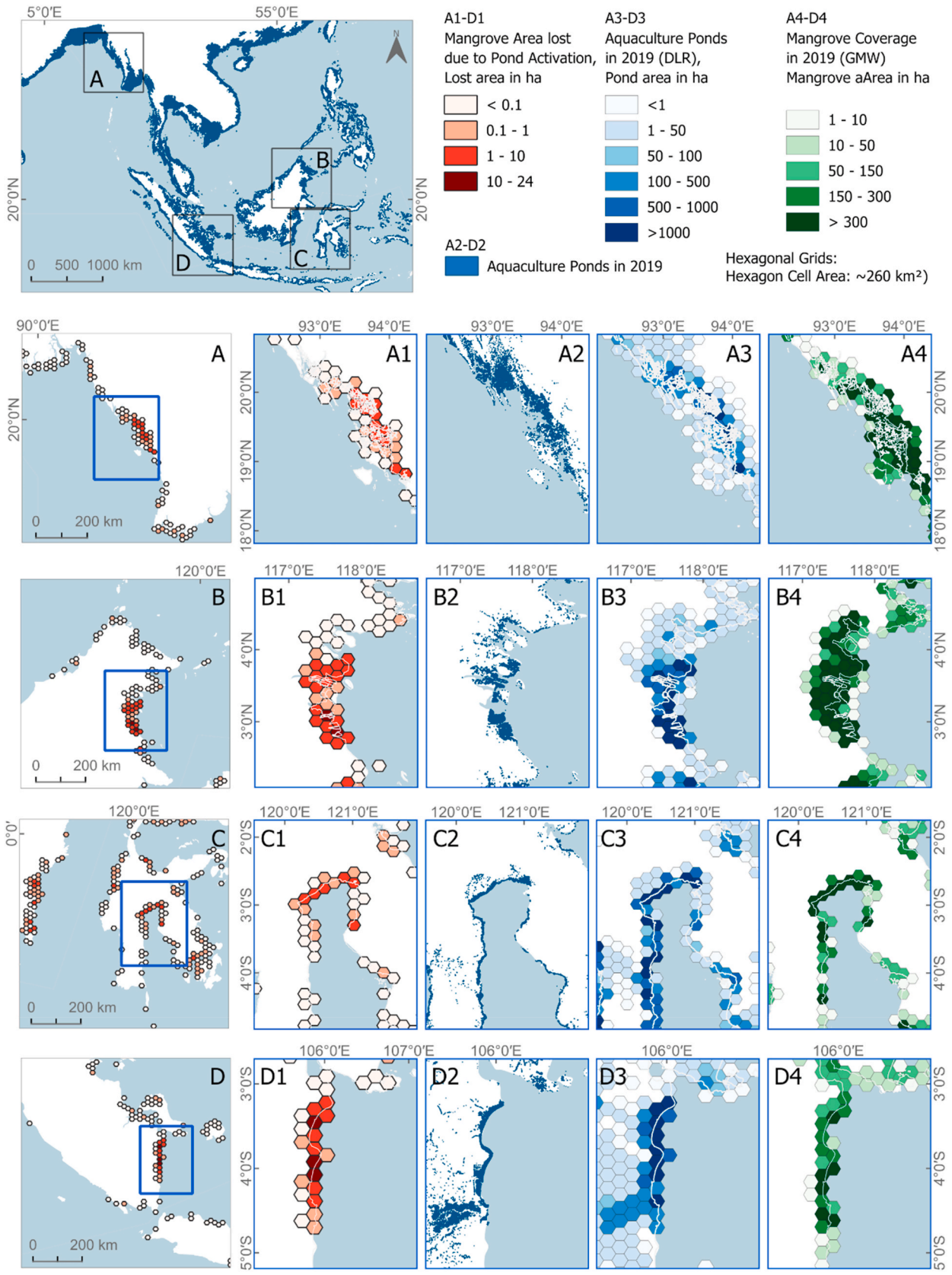


Fig. 12. Spatial patterns of mangrove loss linked to aquaculture pond activation across 4 key Asian coastal regions (A-D). (1) mangrove area lost due to pond activation, (2) pond aquaculture coverage in 2019, (3) pond area in 2019 per hexagon, and (4) mangrove extent in 2019 from the Global Mangrove Watch dataset.

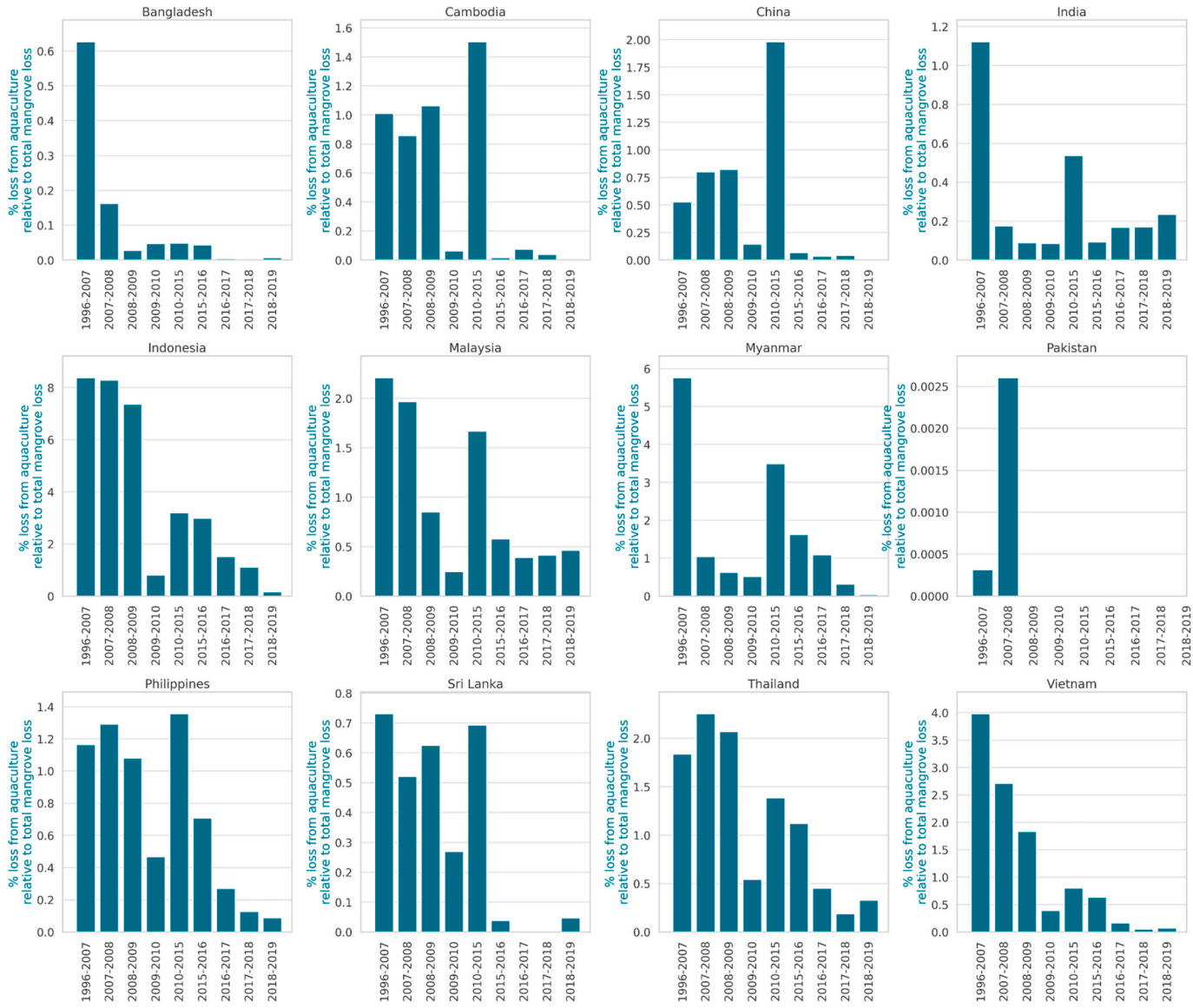


Fig. 13. Percent of loss by aquaculture vs total losses.

contributing essential evidence to guide policies fostering coexistence between economic development and ecosystem protection. This scalable EO-based approach offers a practical basis for identifying priority areas and restoration efforts to safeguard vital coastal mangrove ecosystems.

5. Conclusion

This study offers a comprehensive assessment of the spatial and temporal dynamics between aquaculture pond expansion and mangrove loss across Asia. Indonesia, holding 49.2% of Asia's mangroves in 2020, lost 2284 km^2 (7.2%) from 1996 to 2020, mainly due to aquaculture. Myanmar and Pakistan also faced substantial losses of 564 km^2 (8.9%) and 269 km^2 (22.2%), while Sri Lanka and Iran lost nearly 30% of their mangroves between 1996 and 2019. By integrating a large-scale, high-resolution dataset on pond aquaculture dynamics at a single-object level with mangrove extent data, we have established an effective methodological framework for linking aquaculture expansion to direct mangrove loss. Using a conservative temporal criterion based on positional indices, we successfully linked pond activation events to subsequent mangrove disappearance within a narrow timeframe, thereby minimizing misattribution. The strong positive correlation between aquaculture-driven mangrove loss and the overall decline observed across most countries underscores the critical role of aquaculture in mangrove degradation in Asia. Specifically, Indonesia and Myanmar emerged as major hotspots, losing 13,046 and 2892 ha of mangroves to aquaculture from 1996 to 2007, respectively. While losses declined afterward, Indonesia still lost 5285 ha (2007–2008), and Myanmar saw a resurgence with 1001 ha lost (2010–2015). Other countries like Thailand, Malaysia, and Vietnam experienced moderate losses of 30 to 459 ha per studied period, reflecting regional variability.

This approach improves the detection and interpretation of changes to mangrove ecosystems linked to aquaculture despite uneven temporal sampling, enhancing causal inference. This methodology is transferable to other land cover interactions involving datasets with variable temporal data. Spatial heatmaps and regional analyses emphasize the urgent need for sustainable coastal management strategies that balance aquaculture growth with mangrove conservation. Looking ahead, integrating finer-scale mangrove time series, incorporating uncertainty quantification, and developing automated event detection algorithms will further amplify the analytical power and ecological relevance of the framework. Combining these higher resolution datasets with the presented alignment framework will enable more detailed, timely, and accurate

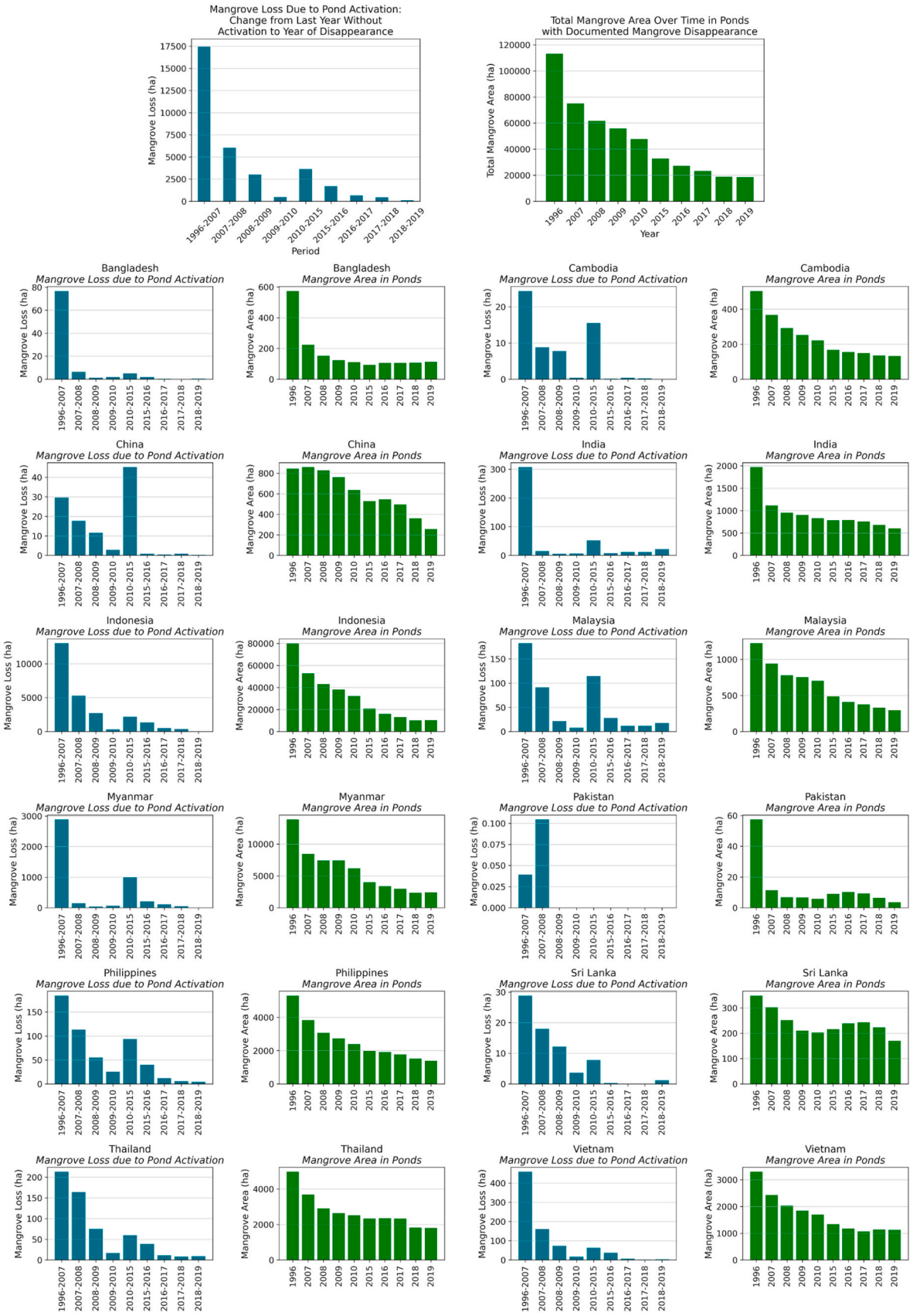


Fig. 14. Mangrove loss due to pond activation and total mangrove area over time for 12 countries. Top row shows overall totals; bottom rows show paired subplots for each country display (left) mangrove loss due to pond activation per period and (right) the total mangrove area in ponds over the years 1996 to 2019.

ecosystem assessments, supporting informed decision-making for coastal resilience and sustainable development. By elucidating the complex interactions between human-driven aquaculture expansion and natural mangrove ecosystems, this research provides vital evidence to inform policy and management decisions.

CRediT authorship contribution statement

Marco Ottinger: Writing – original draft, Visualization, Software, Methodology, Formal analysis, Conceptualization. **Luis David Almeida Famada:** Writing – review & editing, Visualization, Software, Methodology, Formal analysis. **Juliane Huth:** Writing – review & editing, Methodology, Conceptualization.

Software and data processing

The pond dynamics vector dataset, administrative boundary layers, and the Global Mangrove Watch (GMW) dataset were processed using Python (version 3.8). Key libraries included pandas (1.2.2) and geopandas (0.8.2) for data manipulation and spatial operations, geofeather (0.3.0) to efficiently load and analyse large vector datasets. Parallel processing was performed with the multiprocessing package on a CPU server to improve performance and reduce computation time. Python was also used to create line graphs, scatter plots, and pie charts.

Funding

This publication was supported by the open access publication fund of the German Aerospace Center (DLR).

Declaration of competing interest

The authors declare the following financial interests/personal relationships which may be considered as potential competing interests: Marco Ottinger reports article publishing charges was provided by German Aerospace Centre DLR German Remote Sensing Data Center. If there are other authors, they declare that they have no known competing financial interests or personal relationships that could have appeared to influence the work reported in this paper.

Acknowledgements

Special thanks go to the Global Mangrove Watch (GMW) Initiative for the mangrove dataset, the United States Geological Survey (USGS) and the National Aeronautics and Space Administration (NASA) for the Landsat program as well as the European Space Agency (ESA) and the Copernicus Satellite Program for free access to the Landsat archive and Sentinel-1/2 data; and Google Earth Engine team for providing analysis-ready satellite data.

Appendix A. Supplementary data

Supplementary data to this article can be found online at https://doi.org/10.1016/j.ecss.2026.110297.

Data availability

Please contact the authors upon request about the pond data supporting the conclusions of this article.

References

Ahmed, M.U., Alam, MdI., Debnath, S., Debrot, A.O., Rahman, MdM., Ahsan, MdN., Verdegem, M.C.J., 2023. The impact of mangroves in small-holder shrimp ponds in south-west Bangladesh on productivity and economic and environmental resilience. Aquaculture 571, 739464. https://doi.org/10.1016/j.aquaculture.2023.739464.

Akram, H., Hussain, S., Mazumdar, P., Chua, K.O., Butt, T.E., Harikrishna, J.A., 2023. Mangrove health: a review of functions, threats, and challenges associated with mangrove management practices. Forests 14, 1698. https://doi.org/10.3390/f14091698.

Arifanti, V.B., Kauffman, J.B., Subarno, Ilman, M., Tosiani, A., Novita, N., 2022a. Contributions of mangrove conservation and restoration to climate change mitigation in Indonesia. Glob. Change Biol. 28, 4523–4538. https://doi.org/10.1111/gcb.16216.

Arifanti, V.B., Sidik, F., Mulyanto, B., Susilowati, A., Wahyuni, T., Subarno, S., Yulianti, Y., Yuniarti, N., Aminah, A., Suita, E., Karlina, E., Suharti, S., Pratiwi, P., Turjaman, M., Hidayat, A., Rachmat, H.H., Imanuddin, R., Yeny, I., Darwiati, W., Sari, N., Hakim, S.S., Slamet, W.Y., Novita, N., 2022b. Challenges and strategies for sustainable mangrove management in Indonesia: a review. Forests 13, 695. https://doi.org/10.3390/f13050695.

Aslan, A., Rahman, A.F., Robeson, S.M., Ilman, M., 2021. Land-use dynamics associated with mangrove deforestation for aquaculture and the subsequent abandonment of ponds. Sci. Total Environ. 791, 148320. https://doi.org/10.1016/j.scitotenv.2021.148320.

Bunting, P., Rosenqvist, A., Hilarides, L., Lucas, R.M., Thomas, N., Tadono, T., Worthington, T.A., Spalding, M., Murray, N.J., Rebelo, L.-M., 2022. Global Mangrove extent change 1996–2020: Global Mangrove watch version 3.0. Remote Sens. 14, 3657. https://doi.org/10.3390/rs14153657.

Bunting, P., Rosenqvist, A., Lucas, R.M., Rebelo, L.-M., Hilarides, L., Thomas, N., Hardy, A., Itoh, T., Shimada, M., Finlayson, C.M., 2018. The global mangrove watch—A new 2010 global baseline of mangrove extent. Remote Sens. 10, 1669. https://doi.org/10.3390/rs10101669.

Chatting, M., Al-Maslamani, I., Walton, M., Skov, M.W., Kennedy, H., Husrevoglu, S., Le Vay, L., 2024. Past, present and future global mangrove primary productivity. Sci. Total Environ. 957, 177446. https://doi.org/10.1016/j.scitotenv.2024.177446.

Du, C., Khan, S., Ke, Y., Zhou, D., 2023. Assessment of spatiotemporal dynamics of mangrove in five typical mangrove reserve wetlands in Asia, Africa and Oceania. Diversity 15, 148. https://doi.org/10.3390/d15020148.

FAO, 2023. The World's Mangroves 2000–2020. FAO, Rome, Italy. https://doi.org/10.4060/cc7044en.

Friess, D.A., Rogers, K., Lovelock, C.E., Krauss, K.W., Hamilton, S.E., Lee, S.Y., Lucas, R., Primavera, J., Rajkaran, A., Shi, S., 2019. The state of the world's mangrove forests: past, present, and future. Annu. Rev. Environ. Resour. 44, 89–115. https://doi.org/10.1146/annurev-environ-101718-033302.

GADM, 2012. Global administrative areas (2012). GADM Database of Global Administrative Areas version 2.0. [online].

Giri, C., Ochieng, E., Tieszen, L.L., Zhu, Z., Singh, A., Loveland, T., Masek, J., Duke, N., 2011. Status and distribution of mangrove forests of the world using earth observation satellite data. Global Ecol. Biogeogr. 20, 154–159. https://doi.org/10.1111/j.1466-8238.2010.00584.x.

Goldberg, L., Lagomasino, D., Thomas, N., Fatoyinbo, T., 2020. Global declines in human-driven mangrove loss. Glob. Change Biol. 26, 5844–5855. https://doi.org/10.1111/gcb.15275.

Gorelick, N., Hancher, M., Dixon, M., Ilyushchenko, S., Thau, D., Moore, R., 2017. Google Earth engine: Planetary-scale geospatial analysis for everyone. Rem. Sens. Environ. Big Rem. Sens. Data: Tools Appl. Exper. 202, 18–27. https://doi.org/10.1016/j.rse.2017.06.031.

Hagger, V., Worthington, T.A., Lovelock, C.E., Adame, M.F., Amano, T., Brown, B.M., Friess, D.A., Landis, E., Mumby, P.J., Morrison, T.H., O'Brien, K.R., Wilson, K.A., Zganjar, C., Saunders, M.I., 2022. Drivers of global mangrove loss and gain in social-ecological systems. Nat. Commun. 13, 6373. https://doi.org/10.1038/s41467-022-33962-x.

Jennerjahn, T.C., Gilman, E., Krauss, K.W., Lacerda, L.D., Nordhaus, I., Wolanski, E., 2017. Mangrove ecosystems under climate change. In: Rivera-Monroy, V.H., Lee, S. Y., Kristensen, E., Twilley, R.R. (Eds.), Mangrove Ecosystems: a Global Biogeographic Perspective: Structure, Function, and Services. Springer International Publishing, Cham, pp. 211–244. https://doi.org/10.1007/978-3-319-62206-4_7.

Jia, M., Wang, Z., Mao, D., Ren, C., Song, K., Zhao, C., Wang, C., Xiao, X., Wang, Y., 2023. Mapping global distribution of mangrove forests at 10-m resolution. Sci. Bullet. 68, 1306–1316. https://doi.org/10.1016/j.scib.2023.05.004.

Kuenzer, C., Bluemel, A., Gebhardt, S., Quoc, T.V., Dech, S., 2011. Remote sensing of mangrove ecosystems: a review. Remote Sens. 3, 878–928. https://doi.org/10.3390/rs3050878.

Lagomasino, D., Fatoyinbo, T., Lee, S., Feliciano, E., Trettin, C., Shapiro, A., Mangora, M. M., 2019. Measuring mangrove carbon loss and gain in deltas. Environ. Res. Lett. 14, 025002. https://doi.org/10.1088/1748-9326/aaf0de.

Leal, M., Spalding, M.D., 2024. The State of the World's Mangroves 2024. Global Mangrove Alliance. https://doi.org/10.5479/10088/119867.

McSherry, M., Davis, R.P., Andradi-Brown, D.A., Ahmadia, G.N., Van Kempen, M., Wingard Brian, S., 2023. Integrated mangrove aquaculture: the sustainable choice for mangroves and aquaculture? Front. For. Glob. Change 6, 1094306. https://doi.org/10.3389/ffgc.2023.1094306.

Ottinger, M., Bachofer, F., Huth, J., Kuenzer, C., 2022. Mapping aquaculture ponds for the coastal zone of Asia with Sentinel-1 and Sentinel-2 time series. Remote Sens. 14, 153. https://doi.org/10.3390/rs14010153.

Ottinger, M., Kuenzer, C., 2020. Spaceborne L-Band synthetic aperture radar data for geoscientific analyses in coastal land applications: a review. Remote Sens. 12, 2228. https://doi.org/10.3390/rs12142228.

Ottinger, M., Liu, K., Ullmann, T., Huth, J., Kuenzer, C., Bachofer, F., 2026. Pond aquaculture dynamics in Asia: satellite time series for analyzing the spatio-temporal development of coastal aquaculture. Aquaculture 610, 742940. https://doi.org/10.1016/j.aquaculture.2025.742940.

Polidoro, B.A., Carpenter, K.E., Collins, L., Duke, N.C., Ellison, A.M., Ellison, J.C., Farnsworth, E.J., Fernando, E.S., Kathiresan, K., Koedam, N.E., Livingstone, S.R., Miyagi, T., Moore, G.E., Nam, V.N., Ong, J.E., Primavera, J.H., Iii, S.G.S., Sanciangco, J.C., Sukardjo, S., Wang, Y., Yong, J.W.H., 2010. The loss of species: mangrove extinction risk and geographic areas of global concern. PLoS One 5, e10095. https://doi.org/10.1371/journal.pone.0010095.

Rodríguez-Rodríguez, A., Palacios, M.M., Wartman, M., P, D., Costa, M., Macreadie, P.I., Rasheed, A.R., 2025. Current trends and future directions for integrating social values into mangrove restoration. Restor. Ecol. 33, e70139. https://doi.org/10.1111/rec.70139.

Romañach, S.S., DeAngelis, D.L., Koh, H.L., Li, Y., Teh, S.Y., Raja Barizan, R.S., Zhai, L., 2018. Conservation and restoration of mangroves: global status, perspectives, and prognosis. Ocean Coast Manag. 154, 72–82. https://doi.org/10.1016/j.ocecoaman.2018.01.009.

Schuerch, M., Spencer, T., Temmerman, S., Kirwan, M.L., Wolff, C., Lincke, D., McOwen, C.J., Pickering, M.D., Reef, R., Vafeidis, A.T., Hinkel, J., Nicholls, R.J., Brown, S., 2018. Future response of global coastal wetlands to sea-level rise. Nature 561, 231–234. https://doi.org/10.1038/s41586-018-0476-5.

Spalding, M., Kainuma, M., Collins, L., 2010. World Atlas of Mangroves. Routledge, London. https://doi.org/10.4324/9781849776608.

Spalding, M.D., Ruffo, S., Lacambra, C., Meliane, I., Hale, L.Z., Shepard, C.C., Beck, M. W., 2014. The role of ecosystems in coastal protection: adapting to climate change and coastal hazards. Ocean Coastal Manage. 90, 50–57. https://doi.org/10.1016/j.ocecoaman.2013.09.007.

Thomas, N., Lucas, R., Bunting, P., Hardy, A., Rosenqvist, A., Simard, M., 2017. Distribution and drivers of global mangrove forest change, 1996–2010. PLoS One 12, e0179302. https://doi.org/10.1371/journal.pone.0179302.

Vo, Q.T., Kuenzer, C., Vo, Q.M., Moder, F., Oppelt, N., 2012. Review of valuation methods for mangrove ecosystem services. Ecol. Indic. 23, 431–446. https://doi.org/10.1016/j.ecolind.2012.04.022.

Zhang, J., Gan, S., Yang, P., Zhou, J., Huang, X., Chen, H., He, H., Saintilan, N., Sanders, C.J., Wang, F., 2024. A global assessment of mangrove soil organic carbon sources and implications for blue carbon credit. Nat. Commun. 15, 8994. https://doi.org/10.1038/s41467-024-53413-z.